

# Satisfying the Fluctuation Theorem in Free Energy Calculations with Hamiltonian Replica Exchange

Matthew A. Wyczalkowski and Rohit V. Pappu  
*Department of Biomedical Engineering and Center for Computational Biology  
Washington University in St. Louis, St. Louis, MO 63130*

A novel error measure, referred to as the hysteresis error, is developed from the Crooks fluctuation theorem to evaluate sampling quality in free energy calculations. Theory and numerical free energy of hydration calculations are used to show that Hamiltonian replica exchange provides a direct route for minimizing the hysteresis error. Replica exchange swap probabilities yield the rate at which the hysteresis error falls with simulation length, and this result can be used to decrease bias and statistical errors associated with free energy calculations based on multicanonical simulations.

PACS numbers:

## I. INTRODUCTION AND OVERVIEW

Free energies of solvation provide quantitative assessments of driving forces for spontaneous processes such as protein folding, binding, self-assembly, and solubility. Formally, the free energy of solvation in the canonical ensemble is the free energy change  $\Delta F$  associated with the transfer of a solute from the gas phase to a fixed position in the solvent [1]. Operationally, one has access to a range of techniques to obtain estimates for  $\Delta F$  [2, 3]. Kirkwood [4] showed that one could introduce arbitrary parameters into potential functions and continuously vary the degree of coupling between specific molecules in a dense fluid. The device of coupling parameters leads to simple expressions for chemical potentials of any component of the fluid. If the component is the solute molecule, which is transferred from the gas phase into the solvent, then a single coupling parameter  $\lambda$ , where  $0 \leq \lambda \leq 1$ , modulates solute-solvent interactions in the system's potential function. The limits  $\lambda = 0$  and  $\lambda = 1$  correspond to the pure solvent and solvent plus fully grown solute, respectively. Intermediate values of  $\lambda$  correspond to potential functions that include only a part of the solute-solvent interactions. The Kirkwood coupling parameter plays a central role in equilibrium methods for calculating  $\Delta F$ . One carries out a series of independent canonical simulations where each simulation is associated with a distinct potential function, characterized by a specific  $\lambda$  value. As it samples the equilibrium ensemble, each simulation generates a series of work values, which are then used to estimate the free energy change across the entire  $\lambda$  schedule.

The multicanonical approach described above takes advantage of the simple formalism developed by Kirkwood for calculating  $\Delta F$ . However, in practice, standard free energy calculations based on multicanonical simulations are plagued by slow convergence and inaccurate estimates of  $\Delta F$  [5]. Errors may be divided into statistical and bias (or finite sampling) errors [6]. The former stem from the fluctuations of the free energy estimator, and can be estimated by block averaging or bootstrap methods [7, 8]. Since the statistical error decreases as the

inverse square root of simulation length, it is frequently used as an indicator of the convergence of the multicanonical simulation. While statistical errors are random fluctuations of short simulation results about some mean value, the bias error is an error of the mean value itself, and it changes with simulation length. As discussed by Zuckerman and Woolf[9], bias errors have two causes: the free energy estimates are nonlinear averages; and, the work distributions on which such estimates are based will typically have long tails which are rarely sampled, and yet these are important to the average. The latter point is important: rare events dominate free energy estimates, and one seldom observes these events in short simulations. As a result, the average drifts with simulation length, resulting in inaccurate estimates for  $\Delta F$  from bias error even when the statistical error is small. The magnitude of the bias error is difficult to quantify directly, as it requires knowledge of the actual free energy difference, the very quantity we wish to determine. Furthermore, small fluctuations in the estimate for  $\Delta F$  may not be indicative of convergence, but rather of inadequate sampling of the rare but important configurations. To address these problems, we develop an alternate measure of free energy error, one based on deviations from equilibrium distributions.

Crooks [10] derived a fluctuation theorem (appendix A 1) valid for stochastic, microscopically reversible dynamics, which relates the distribution of dissipated work values along a forward and reverse path as,

$$\exp(\beta W_D) = \frac{P_F(\beta W_D)}{P_R(-\beta W_D)}. \quad (1)$$

Here,  $\beta = (k_B T)^{-1}$ ,  $P_F(\beta W_D)$  is the probability distribution for dissipated work associated with switching  $\lambda$  from  $\lambda_0$  to  $\lambda_1$ , and  $P_R(-\beta W_D)$  is the corresponding distribution for the reverse process. If the canonical simulations for each value of  $\lambda$  sample the equilibrium ensemble adequately, then the distributions of dissipated work obtained over the course of free energy calculations will satisfy Eq. (1).

In this work, we develop a readily measured error estimate, the hysteresis error  $\epsilon_H$ , which quantifies the

degree to which observed work distributions obey the Crooks fluctuation theorem. Hamiltonian replica exchange, a multicanonical equilibration technique, effectively reduces the hysteresis error. We relate the average replica exchange swap probability to the degree of overlap between equilibrium ensembles, as well as to the rate at which  $\epsilon_H$  falls. Based on this, we may construct an optimized  $\lambda$  schedule to further minimize the hysteresis error for an entire simulation.

The remainder of this presentation is organized as follows: the theory section introduces the hysteresis error in the context of the Crooks fluctuation theorem followed by a formal illustration of how Hamiltonian replica exchange minimizes  $\epsilon_H$ ; the definition of swap probability as a measure of the overlap between different equilibrium ensembles; and a connection between the amount of overlap and minimization of  $\epsilon_H$ . We calculate the free energy of hydration for acetamide to demonstrate how to estimate  $\epsilon_H$  and minimize this error using replica exchange coupled to standard multicanonical simulations. We conclude with a summary and a discussion of the features of our methodology.

## II. THEORY

### A. Background

The free energy of replica  $i$  in the canonical ensemble at temperature  $T$ , whose potential  $U_i(\Gamma) = U(\Gamma, \lambda_i)$  is a function of system configuration  $\Gamma$  and the parameter  $\lambda_i$ , is formally given as [11],

$$F_i = \beta^{-1} \ln \left\{ \int d\Gamma \exp[-\beta U_i(\Gamma)] \right\}. \quad (2)$$

At equilibrium, the probability of observing configuration  $\Gamma$  is given as,

$$\rho_i(\Gamma) = \exp\{\beta[F_i - U_i(\Gamma)]\}. \quad (3)$$

To calculate the free energy change  $\delta F$  associated with switching the Hamiltonian from  $U_0$  to  $U_1$  we perform simulations at  $\lambda_0$  and  $\lambda_1$ , and calculate the forward and reverse work as,

$$W^F(\Gamma) = U_1(\Gamma) - U_0(\Gamma), \quad (4a)$$

$$W^R(\Gamma) = U_0(\Gamma) - U_1(\Gamma). \quad (4b)$$

For the forward and reverse work values the configuration  $\Gamma$  is typically drawn from the equilibrium ensemble of  $U_0$  and  $U_1$ , respectively. The Free Energy Perturbation (FEP) method [12] utilizes forward and reverse work distributions to provide two independent estimators for  $\delta F$ ,

$$\delta F_{FEP}^F = -\beta^{-1} \ln \langle \exp(-\beta W^F) \rangle_0, \quad (5a)$$

$$\delta F_{FEP}^R = +\beta^{-1} \ln \langle \exp(-\beta W^R) \rangle_1, \quad (5b)$$

where the forward estimator  $\delta F_{FEP}^F$  utilizes forward work values from the simulation at  $U_0$ , and the reverse estimator the reverse work from  $U_1$ . Note that in both cases  $\delta F$  is associated with the process of switching  $\lambda_0 \rightarrow \lambda_1$ . These two estimators have different convergence rates [6]. Therefore, while in practice the two estimates should be equal, in simulations with finite sampling they are generally different.

Another free energy estimator, the Bennett Acceptance Ratio [13], uses both the  $W^F$  and  $W^R$  distributions to obtain a free energy estimate. It is generally more accurate [14] and is employed later in this paper for numerical free energy estimates, but will not be considered for theoretical development.

### B. The Hysteresis Error

The hysteresis error  $\epsilon_H$  is defined as the difference between the forward and reverse  $\delta F_{FEP}$  estimates,

$$\epsilon_H \equiv \delta F_{FEP}^F - \delta F_{FEP}^R. \quad (6)$$

$\epsilon_H$  has contributions from both the statistical and bias error of the FEP estimators [6, 9]. The bias error of the two estimators is typically in the opposite direction. While the statistical error may dominate the  $\epsilon_H$  for a given simulation, in averages over multiple short simulations the dominant contribution to the average hysteresis error is the sum of the forward and reverse FEP bias.

We take  $\epsilon_H$  as a measure of sampling quality and aim to minimize its magnitude between all pairs of neighboring replicas. The validity of using  $\epsilon_H$  as a general sampling error is based on a relationship between it and the fluctuation theorem of Crooks(1), derived below.

Switching the parameter  $\lambda_0 \rightarrow \lambda_1$  (and vice versa) is equivalent to performing non-equilibrium work; the difference between the work performed and the free energy change of the system is the dissipated work, defined in the forward and reverse direction as,

$$W_D^F(\Gamma) = W^F(\Gamma) - \delta F, \quad (7a)$$

$$W_D^R(\Gamma) = W^R(\Gamma) + \delta F. \quad (7b)$$

Crooks [10] equates  $W_D^F$  and  $W_D^R$  to the entropy production caused by changing  $\lambda_0 \rightarrow \lambda_1$  and  $\lambda_1 \rightarrow \lambda_0$ , respectively, for the given configuration.

The distributions  $P_F(W_D)$  and  $P_R(W_D)$  give the probability of realizing a specific value for the dissipated work in the forward and reverse directions, respectively. The distributions are related to each other by the fluctuation theorem shown in Eq. (1), which we have re-derived in appendix A 1 for the specific case of instantaneous switching between configurations with different  $\lambda$  values. In practice, Eq. (1) will not be satisfied exactly because of errors due to finite sampling. To take simulation errors into account, we rewrite Eq. (1) with an arbitrary error

term  $\epsilon_{FT}^*$  and with observed (rather than ideal) dissipated work distributions  $P_F^*$  and  $P_R^*$ ,

$$\exp[\beta W_D + \beta \epsilon_{FT}^*(W_D)] = \frac{P_F^*(\beta W_D)}{P_R^*(-\beta W_D)}. \quad (8)$$

Eq. (8) is constructed such that the Crooks fluctuation theorem is recovered and  $\epsilon_{FT}^* = 0$  when the observed work distributions match the correct distributions. The hysteresis error  $\epsilon_H$  and the fluctuation error  $\epsilon_{FT}^*$  are related to each other as, (see appendix A 2),

$$\epsilon_H = -\beta^{-1} \ln \langle \exp(-\beta \epsilon_{FT}^*) \rangle_0^*, \quad (9)$$

where  $\langle \cdot \rangle^*$  is defined as the average obtained from a finite simulation. The more closely a simulation obeys the relationship (1), the smaller the hysteresis error  $\epsilon_H$ , and vice versa. In the next section, we will discuss methods to reduce  $\epsilon_H$ , which in turn leads to the satisfaction of the Crooks fluctuation theorem.

### C. Replica Exchange

In a Hamiltonian replica exchange [15, 16] simulation, Monte Carlo moves are employed to exchange configurations  $\Gamma$  (or equivalently, parameters  $\lambda$ ) between two replicas with the probability,

$$P_{swap} = \min[1, \exp(-\beta \Delta U_{swap})], \quad (10)$$

where,

$$\Delta U_{swap} = U_0(\Gamma_1) + U_1(\Gamma_0) - U_0(\Gamma_0) - U_1(\Gamma_1), \quad (11a)$$

$$= W^F + W^R, \quad (11b)$$

$$= W_D^F + W_D^R. \quad (11c)$$

$\Gamma_0$  and  $\Gamma_1$  denote configurations drawn at random from the equilibrium ensembles of  $U_0$  and  $U_1$ , respectively. For convenience, we write  $\gamma = (\Gamma_0, \Gamma_1)$  as a pair of such configurations, and  $\gamma' = (\Gamma_1, \Gamma_0)$  is the swapped configuration pair.

Since  $\Gamma_0$  and  $\Gamma_1$  are independent configurations, we can consider the probability of sampling  $\Gamma_0$  in the equilibrium ensemble of  $U_0$  and sampling  $\Gamma_1$  in the equilibrium ensemble of  $U_1$ ; this is the native probability  $\rho_N(\gamma)$ . Analogously, the joint probability of sampling the swapped configurations,  $\Gamma_1$  from  $\rho_0$  and  $\Gamma_0$  from  $\rho_1$  is given as  $\rho'_N(\gamma)$ :

$$\rho_N(\gamma) = \rho_0(\Gamma_0)\rho_1(\Gamma_1), \quad (12a)$$

$$\rho'_N(\gamma) = \rho_0(\Gamma_1)\rho_1(\Gamma_0) = \rho_N(\gamma'). \quad (12b)$$

Replica exchange swaps are conveniently visualized by plotting the independent configurations  $\Gamma_0$  and  $\Gamma_1$  along orthogonal axes and the equilibrium ensemble of the system as an isocontour of  $\rho_N$ , illustrated in Fig. 1(a).

At equilibrium, the relative probability of observing a pair of replicas in their swapped versus native configurations is,

$$\frac{\rho'_N}{\rho_N} = \exp(-\beta \Delta U_{swap}), \quad (13)$$

which is derived with definitions (12), (3) and (11a). We will refer to this as an inter-replica equilibrium relationship.

In an infinitely long simulation, (13) will be satisfied exactly, but this will generally not be the case for finite simulations, where inadequate sampling of configuration space will result in inaccurate probability estimates. However, in simulations with replica exchange we expect the inter-replica equilibrium relationship to be satisfied more closely than in simulations without replica exchange, because the swap move distributes configuration pairs in such a way as to satisfy Eq. (13). To illustrate, consider the system in Fig. 1(a) where the  $U_0$  replica is presumed to be stuck in the left lobe of the  $\rho_0$  distribution because of a kinetic barrier. Without replica exchange, only the shaded region of  $\rho_N$  will be sampled accurately. The simulation will not have a correct estimate for  $\rho'_N(\gamma_c) = \rho_N(\gamma'_c)$ , since  $\rho_0$  for the swapped configuration, never having been observed, will be inaccurate. Consequently, Eq. (13) will not hold. Replica exchange directly populates swapped configurations (e.g.,  $\gamma'_c$ ), thereby improving the statistics of  $\rho'_N$  and allowing inter-replica equilibrium to be achieved more quickly for all configurations in  $\rho_N$ .

The degree to which Eq. (13) is satisfied determines the magnitude of the hysteresis error. To illustrate this, suppose that the distribution  $\rho'_N$  has some small error  $\rho_\epsilon(\Gamma_0, \Gamma_1)$  due to finite sampling, so that we write  $(\rho'_N + \rho_\epsilon)$  as the numerator in Eq. (13). In appendix A 3 we show, by integrating over all configuration pairs, that the relationship between the hysteresis error and the error of sampling the swapped distribution,  $\rho_\epsilon$  is,

$$\epsilon_H \simeq -\beta^{-1} \int d\Gamma_0 d\Gamma_1 \rho_\epsilon. \quad (14)$$

The hysteresis error, then, will be minimized when the estimated swapped configuration probabilities  $\rho'_N$  are consistent with the equilibrium distribution. Since replica exchange populates the swapped configurations directly, it provides an efficient route to minimizing  $\epsilon_H$ .

### D. Swap Probability

Analysis of the average swap probability is complicated by the fact that the Metropolis function (Eq. (10)) is not analytical. For the purposes of interpreting this quantity, we will instead consider the Fermi swap probability,

$$p_{swap} = f(\beta \Delta U_{swap}),$$

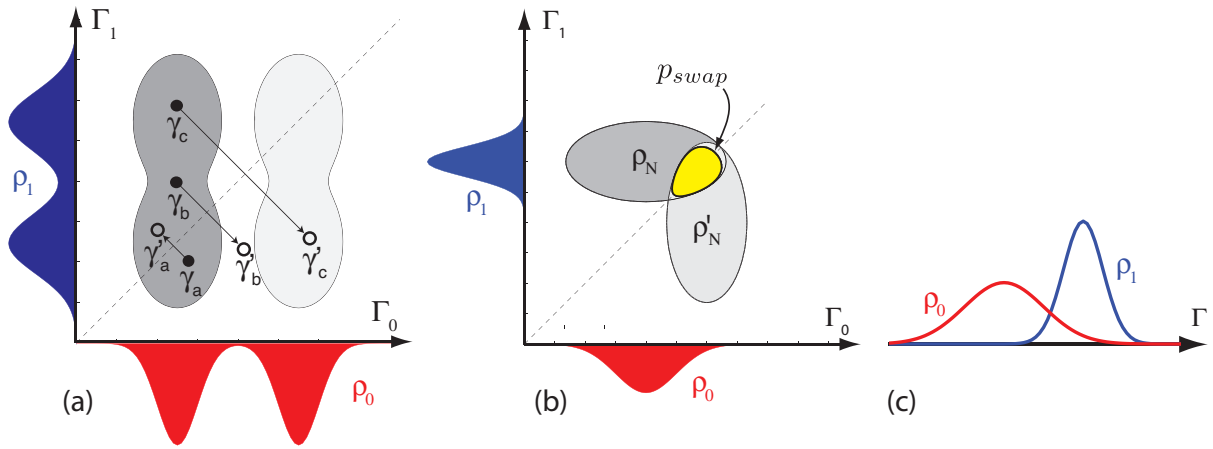


FIG. 1: A graphical representation of replica exchange. **(a)** The independent (high dimensional) configuration spaces  $\Gamma_0$  and  $\Gamma_1$  have probability distributions  $\rho_0$  and  $\rho_1$ , respectively, and the joint equilibrium ensemble  $\rho$  is drawn over this domain. The  $\rho_0$  system has a kinetic barrier (represented by the two disconnected lobes) and with no replica exchange the system explores only the configurations of the shaded domain. A replica exchange swap is a reflection of the configuration pair  $\gamma$  about the  $\Gamma_0 = \Gamma_1$  diagonal axis, and three swap attempts are shown: the configuration pair  $\gamma_a$  swaps successfully and becomes  $\gamma'_a$ , but it does not sample otherwise inaccessible regions; a swap of  $\gamma_b$  fails because  $\gamma'_b$  is not in the equilibrium ensemble; and the swap of  $\gamma_c$  succeeds and allows the system to explore otherwise inaccessible regions of phase space. **(b)** The equilibrium domain  $\rho_N$  and its swapped image  $\rho'_N$  are drawn. Swaps are feasible only for configuration pairs which belong to both  $\rho_N$  and  $\rho'_N$ . This overlap region, labeled  $p_{swap}$ , is the domain where the integrand of Eq. (17b) is large, and its size corresponds to the average swap probability. **(c)** The overlap of the  $\rho_0$  and  $\rho_1$  distributions along the common configuration  $\Gamma_0 = \Gamma_1$ . For the hysteresis error to converge, the  $\lambda_0$  simulation must observe configurations where  $\rho_1 > \rho_0$ , and the  $\lambda_1$  simulation must adequately sample the region  $\rho_0 > \rho_1$ . The frequency with which this occurs is given by  $\langle p_{swap} \rangle$ .

where  $f(x)$  is defined as,

$$f(x) = 1/[1 + \exp(x)]. \quad (15)$$

(See [13] for discussion). We use  $p_{swap}$  to denote the Fermi swap probability and  $P_{swap}$  for the Metropolis swap probability; while the theoretical development uses  $p_{swap}$ , replica exchange moves are accepted/rejected using  $P_{swap}$ . A simulation with either the Metropolis or Fermi swap probability will yield a Boltzmann distribution of swapped and unswapped configurations (Eq. (13)). While the exact numerical values of the Fermi and Metropolis swap probabilities will differ somewhat, their qualitative behavior and the conclusions drawn here will hold for both.

The average Fermi swap probability for two systems evolving independently is,

$$\langle p_{swap} \rangle \equiv \langle \langle f(\beta \Delta U_{swap}) \rangle \rangle_1, \quad (16a)$$

$$= \int d\Gamma_0 d\Gamma_1 \rho_N f(\beta \Delta U_{swap}), \quad (16b)$$

which can be written as,

$$\langle p_{swap} \rangle = \left\langle \left\langle \frac{\rho'_N}{\rho_N + \rho'_N} \right\rangle \right\rangle_1, \quad (17a)$$

$$= \int d\Gamma_0 d\Gamma_1 \frac{\rho_N \rho'_N}{\rho_N + \rho'_N}. \quad (17b)$$

The integrand of (17b) is a normalized probability of observing a given configuration pair, and the average swap probability is then the overlap of  $\rho_N$  and  $\rho'_N$ . See Fig. 1(b) for a graphical interpretation. Thus, a large average swap probability implies a large overlap between the equilibrium distributions of the two replicas, and a low  $\langle p_{swap} \rangle$  indicates that the configurations these replicas adopt are distinct.

We can expand (16a) in a Taylor series about  $\lambda = \lambda_0 + \delta\lambda$ . To leading order in  $\delta\lambda$ , we find that in the neighborhood of  $\lambda_0$  the average swap probability is, (see appendix A 4),

$$\langle p_{swap} \rangle \simeq \frac{1}{2} - \frac{\beta^2 \delta\lambda^2}{4} C_\lambda, \quad (18)$$

where

$$C_\lambda \equiv \text{var} \left( \frac{\partial U}{\partial \lambda} \right) = \langle (\partial U / \partial \lambda)^2 \rangle_0 - \langle \partial U / \partial \lambda \rangle_0^2.$$

$C_\lambda$ , then, determines the rate at which the average swap probability declines as the difference in  $\lambda$  between the two replicas,  $\delta\lambda$ , increases, although this linear analysis is accurate only for small  $\delta\lambda$ .

### E. Swap Probability and the Hysteresis Error Convergence Rate

We now demonstrate that the average swap probability between two replicas gives a measure of how quickly the hysteresis error decreases, on average, over the course of a simulation. The hysteresis error is the difference between the forward and reverse  $\delta F_{FEP}$ , and since the forward and reverse FEP estimators do not converge at equal rates [6], it is the slower of these which governs the convergence of  $\epsilon_H$ .

We may rewrite Eq. (5a) as,

$$\langle \exp(-\beta W_D^F) \rangle_0 = 1. \quad (19)$$

For this to hold, we must sample configurations where  $W_D^F < 0$ ; since the dissipated work is on average greater than zero by the second law of thermodynamics, such configurations tend to be rare [17]. As a result, the convergence rate of  $\delta F_{FEP}^F$  is governed by the probability of observing negative dissipated forward work values. Likewise, the convergence of  $\delta F_{FEP}^R$  is dictated by observations of  $W_D^R < 0$ . We can understand this criterion graphically with the relationships, (see appendix A 1),

$$\frac{\rho_0(\Gamma_0)}{\rho_1(\Gamma_0)} = \exp[\beta W_D^F(\Gamma_0)], \quad (20a)$$

$$\frac{\rho_1(\Gamma_1)}{\rho_0(\Gamma_1)} = \exp[\beta W_D^R(\Gamma_1)]. \quad (20b)$$

In the context of Fig. 1(c), observing  $W_D^F < 0$  corresponds to sampling configurations from the  $\rho_0$  distribution where  $\rho_1 > \rho_0$ , and for  $W_D^R < 0$  we require  $\rho_0 > \rho_1$  when sampled from the  $\rho_1$  distribution.

Turning our attention to the average swap probability, we note that  $\Delta U_{swap}$ , which is the sum of  $W_D^F$  and  $W_D^R$ , is negative whenever  $\rho'_N > \rho_N$  (by Eq. (13)). Configurations for which this is the case are sampled by a simulation only in the lower-right half of the domain labeled  $p_{swap}$  in Fig. 1(b). The larger this domain, whose size is given by the average swap probability, the more frequently negative values of  $W_D^F$  and  $W_D^R$  are observed, and the more quickly the hysteresis error converges. A numerical confirmation of this argument, that low swap probabilities correspond to large hysteresis errors and vice versa, is demonstrated in the results section.

### III. METHODS

The computational system consists of 21 replicas, each with a different  $\lambda$ , which are simulated independently to obtain equilibrium statistics. The parameter  $\lambda$  controls the non-bonded interactions between an acetamide (ACE) solute and the water molecules. Two independent sets of simulations were performed, with and without replica exchange, in order to investigate the effect of this technique.

The Lennard-Jones and Coulomb interactions between the water and ACE molecules are scaled by  $\lambda_{LJ}$  and  $\lambda_C$ , respectively. We scaled both parameters simultaneously, such that  $\lambda_{LJ} = \lambda_C$ ; the single parameter  $\lambda$  then refers to both terms. The specific way in which the Lennard-Jones and Coulomb terms scale with  $\lambda$  is described in appendix B.  $\lambda$  varies across the 21 replicas from 0 to 1 in increments of 0.05.

Each replica consists of 343 water molecules and one ACE molecule, which is rigid and whose position is fixed in the central box. All simulations were performed at constant temperature (298K) and volume (21.8Å cubic box) using Metropolis Monte Carlo sampling. Parameters from the OPLS-AA force field [18] and 4-site TIP4P water model [19] were used to model the solute and solvent, respectively. Minimum image boundary conditions and spherical cutoffs were employed for the Coulomb and Lennard-Jones potentials. The cutoff radius was 10.5Å for electrostatic interactions and 10Å for van der Waals interactions. Cutoffs were group-based for the former, and atom-based for the latter. No long-range corrections were employed. All simulations were carried out using the MCCC'S Towhee [20] Monte Carlo simulation package[32].

The initial configurations for all replicas were identical and correspond to the end-point of a pre-equilibration run with ACE in water. For each replica, simulations consisted of 2 million cycles, where a cycle corresponds to 343 Monte Carlo moves; each move combines rotations and translations of a randomly chosen individual water molecule. The initial  $10^5$  cycles were discarded for equilibration. The average acceptance rate for all replicas was 31%.

The replica exchange simulation consists of a number of simulation rounds, where each replica evolves independently, separated by swap rounds, when a number of swap attempts take place. The length of the simulation round was drawn from a normal distribution with a mean of 500 and standard deviation of 50 cycles. 500 cycles is the approximate energy autocorrelation “time”. The swap round consists of  $21^2$  swap attempts between randomly selected replica pairs. Allowing swaps beyond neighboring replicas increases the efficiency of replica exchange, by allowing a replica to traverse the entire range of  $\lambda$  from 0 to 1 more quickly than if only neighbor swaps were permitted [21].

During the course of the simulation, the native ( $U_i(\Gamma_i)$ ) and foreign ( $U_{j \neq i}(\Gamma_i)$ ) potential energies, as well as values for  $dU/d\lambda_C$  and  $dU/d\lambda_{LJ}$  (where  $dU/d\lambda = dU/d\lambda_{LJ} + dU/d\lambda_C$ ), were saved every 10 cycles. These were then post-processed to obtain the free energies, the hysteresis error, swap probabilities, and  $C_\lambda$ , regardless of whether actual replica exchange swaps took place. The total free energy of hydration,  $\Delta F$ , is the sum of all free energy changes  $(\delta F)_i$  between neighboring replicas  $i$  and  $i + 1$ , calculated using the Bennett Acceptance Ratio

method [13],

$$\Delta F \equiv \sum_i^{M-1} (\delta F)_i$$

where  $M$  is the total number of replicas. Similarly, the RMS hysteresis error  $\epsilon_{RMS}$  is the root-mean-square of the hysteresis error  $(\epsilon_H)_i$  between neighboring replicas,

$$\epsilon_{RMS} \equiv \sqrt{\sum_i^{M-1} (\epsilon_H)_i^2 / M}$$

Statistical errors for  $\Delta F$  were estimated using the bootstrap method [8]. With the simulation dataset consisting of  $N$  observations, we drew  $n^*$  observations at random and with replacement to create one bootstrap estimate,  $\Delta F^*$ . This process was repeated 10,000 times, and the standard deviation among all the  $\Delta F^*$  is the estimated error of  $\Delta F$ .  $n^*$  is the expected number of independent observations in the dataset; here,  $n^* = 1900$  with the assumption that there is one independent observation per two internal energy autocorrelation “times” [22].

## IV. RESULTS

### A. Acetamide Free Energy of Hydration

The hydration free energies we calculate for acetamide are in line with results obtained by other researchers, as shown in Table I. All numerical results differ somewhat from experimental values due to differences in force field parameters. Our calculations were carried out in the canonical ensemble. Therefore, we obtain estimates for the Helmholtz free energy  $\Delta F$ , whereas the experimental and other computational values obtain estimates for the Gibbs free energy,  $\Delta G$ . However, the distinction between these two values should be negligible [23]. The consistency between our results and those of others serves to verify our implementation and sampling technique.

Table I shows differences between results obtained with and without replica exchange. As expected from our theoretical considerations, we find that the RMS hysteresis error is lowered by an order of magnitude when replica exchange is coupled to the multicanonical sampling protocol. However, it should be noted that the statistical error estimated using bootstrap remains unaffected. This is not an artifact of the bootstrap method used to estimate statistical errors. Instead, fluctuations in estimates for  $\delta F$  originate in fluctuations of the underlying work distribution, shown in Eq. (1). So long as both simulations sample the work distribution adequately, they will have similar statistical error associated with them. As a cautionary note, low statistical errors can also be caused by inadequate sampling of the appropriate work distributions. The statistical error between two replicas can

be reduced by decreasing the  $\lambda$ -distance between them, and an optimal  $\lambda$  schedule can reduce it for an entire simulation.

### B. Hysteresis Error and Replica Exchange

For a fixed  $\lambda$  schedule, the hysteresis error may be reduced with either an improved sampling methodology like replica exchange, or longer simulations per replica. The effects of both approaches are illustrated in Fig. 2.

Panel (a) shows  $\epsilon_H$  for each neighboring replica pair. The hysteresis error is not uniform across all pairs, with spikes in the region  $\lambda = 0.1 - 0.3$ . Replica exchange systematically reduces the hysteresis error for all pairs of replicas.

Panel (b) illustrates how both longer sampling and replica exchange affect the hysteresis error. Block averaging shows that the average RMS hysteresis error declines consistently with longer simulations. This reduction can be improved with replica exchange; in fact, a simulation with replica exchange will achieve the same magnitude of RMS hysteresis error 5 times more quickly than one without replica exchange.

### C. Average Swap Probability

Fig. 3 shows downward spikes in the swap probability for values of  $\lambda$  where the hysteresis error is large in Fig. 2(a). These results are consistent with the proposal that swap probability between two replicas is an indicator of the rate at which  $\epsilon_H$  is minimized. The same region is characterized by a positive spike in  $C_\lambda$ , which is expected based on the relationship between the swap probability and  $C_\lambda$  in Eq. (18). However, while the swap probability calculation requires two separate simulations, estimates of  $C_\lambda$  can be obtained from just one. Moreover,  $\langle p_{swap} \rangle$  varies as the distance between the replicas changes, complicating the interpretation if the  $\lambda$  schedule is not uniform. Evaluation of  $C_\lambda$  as a function of  $\lambda$  using a preliminary, coarse  $\lambda$  schedule can identify regions where the swap probability is expected to be low, and can be used to construct optimal  $\lambda$  schedules, as discussed in Sec. VB.

## V. DISCUSSION

### A. Physical Interpretation of $C_\lambda$ Profile

To gain a physical interpretation of the profile for  $C_\lambda$  shown in Fig. 3, we plot in Fig. 4 the average water density in a  $2.5\text{\AA}$  sphere surrounding the carbonyl carbon of acetamide. The plot shows that water occupancy around the growing solute decreases rapidly in the range of  $\lambda \sim 0.15$ . The expulsion and rearrangement of water molecules during cavitation leads to a large shift in the

**(a) Acetamide Free Energy of Hydration: Current Work**

	$\Delta F$ (kcal/mol)	$\epsilon_{RMS}$ (kcal/mol)
No Replica Exchange	$-8.35 \pm 0.051$	0.120
Replica Exchange	$-8.14 \pm 0.053$	0.023

**(b) Acetamide Free Energy of Hydration: Literature**

	$\Delta G$ (kcal/mol)	Details
MacCallum and Tieleman [24]	$-8.25 \pm 0.26$	TIP4P, TI
Shirts <i>et al.</i> [25]	$-8.20^a \pm 0.03$	TIP3P, TI
Chang <i>et al.</i> [26]	$-8.54 \pm 0.1 - 0.3$	TIP4P, BAR
Udier-Blagović <i>et al.</i> [27]	$-9.65 \pm 0.3 - 0.5$	TIP4P, FEP
Experimental [28]	-9.54	

<sup>a</sup>No long range van der Waals corrections

TABLE I: The hydration free energy of acetamide. **(a)** The Helmholtz hydration free energy  $\Delta F$  for the current work, as calculated by the Bennett Acceptance Ratio, and the RMS hysteresis error. The  $\Delta F$  statistical errors are calculated by the bootstrap method. **(b)** Published values of the Gibbs free energy  $\Delta G$ , obtained both computationally and experimentally. All computational results utilize the OPLS-AA force field for the solute acetamide. Also noted are the water model and free energy estimator (TI: Thermodynamic Integration; FEP: Free Energy Perturbation; BAR: Bennett Acceptance Ratio)

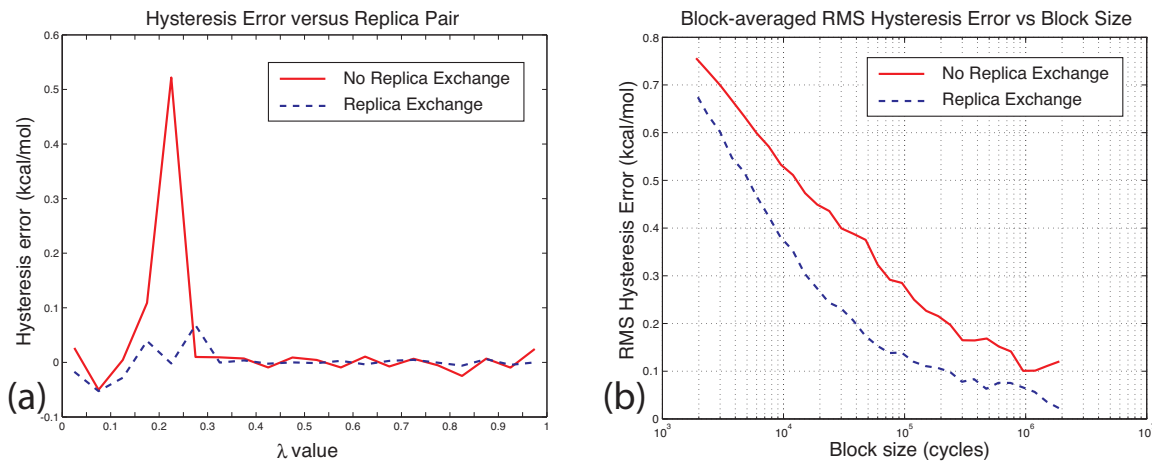


FIG. 2: **(a)** The hysteresis error between neighboring replicas. Replica exchange effectively reduces the hysteresis error for replica pairs. **(b)** Block averages of the RMS hysteresis error, showing that the hysteresis error falls with increasing block size. Replica exchange increases the rate at which hysteresis error is lowered, thereby achieving the same magnitude error with simulations which are on average 4-8 times shorter.

equilibrium ensemble, giving rise to a pronounced spike in  $C_\lambda$ . (Smaller shifts in  $C_\lambda$  near  $\lambda = 1$  reflect electrostatic effects and are not observed for simulations where  $\lambda_C = 0$ , data not shown.) Thus,  $C_\lambda$  profiles serve as useful probes for detecting large shifts in equilibrium ensembles. Regions where the equilibrium ensembles change most rapidly are the regions that contribute to the largest errors in free energy calculations.

### B. Optimal $\lambda$ Schedule for Free Energy Calculations

For given computational resources, with the number of replicas and the simulation length fixed, the RMS hys-

teresis error of a simulation may be decreased by optimizing the  $\lambda$  schedule, or the distribution of  $\lambda$  across the replicas. The swap probability gives the rate at which the average hysteresis error falls between two replicas, and in an optimized simulation it would be uniform across all replica pairs. In practice it is difficult to obtain the  $\lambda$  schedule which makes the swap probability exactly uniform, but reasonable approximations can be made by using the linearized swap probability, given by Eq. (18).

First, it is necessary to perform some number of preliminary simulations to obtain  $C_\lambda$  along a coarse  $\lambda$  schedule. These initial simulations need not be as long as the final production runs, since  $C_\lambda$  converges more quickly than  $\delta F$  and is more tolerant of error. With a rough estimate of  $C_\lambda(\lambda)$  in hand, the  $\lambda$  schedule can be adjusted to en-

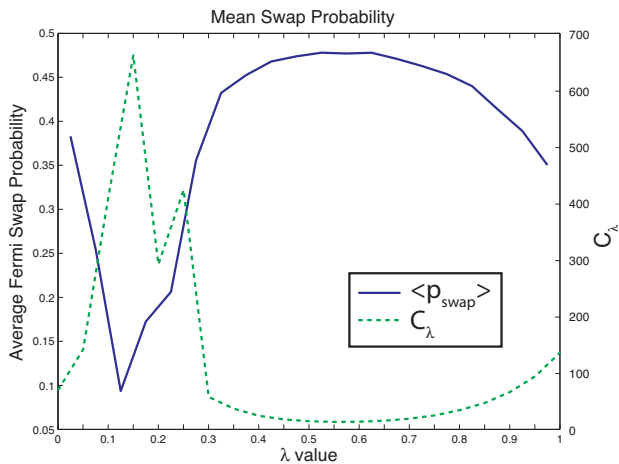


FIG. 3: The average swap probability between adjacent replicas and  $C_\lambda = \text{var}(\partial U / \partial \lambda)$  evaluated for each replica (from the replica exchange simulation; simulation with no replica exchange is not significantly different). Spikes in  $C_\lambda$  indicate regions of low swap probability.

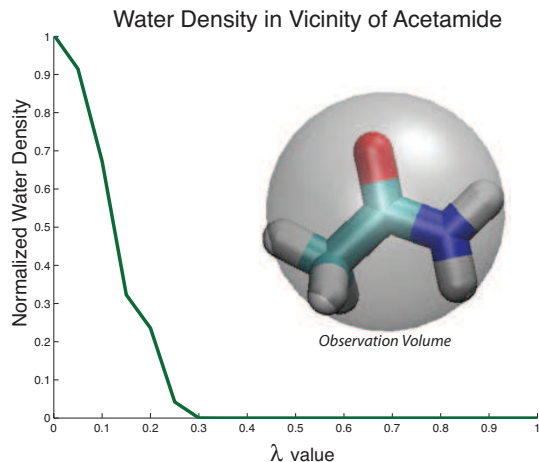


FIG. 4: Water density within  $2.5\text{\AA}$  of the acetamide carbonyl carbon as  $\lambda$  varies. The inset illustrates the position and size of the observation volume with respect to an ACE molecule. Density is normalized by the bulk density. As  $\lambda$  increases, waters are expelled by the growing cavity.

sure that the linear swap probability is uniform between all replicas. Alternatively, one might simply shift replicas from where  $C_\lambda$  is small to where it is large. Both approaches are only approximate, and break down when the linear response assumption in Eq. (18) ceases to be valid. They may be applied iteratively as  $C_\lambda$  is evaluated for new  $\lambda$  schedules.

The aim of an optimal  $\lambda$  schedule is to place replicas close together in regions where the  $C_\lambda$  profile shows spikes. This ensures reasonable swap probabilities and minimal hysteresis errors in regions that are problem-

atic. Preliminary investigations show that even when the schedule is improved in an *ad hoc* manner, hysteresis as well as statistical errors decrease.

### C. Replica Exchange

Replica exchange provides a Monte Carlo move which may allow a replica to access a distant part of its equilibrium ensemble in one step. It is no substitute for conformational exploration within a replica. This point, while obvious, must be emphasized in the context of the hysteresis error, which does not report on the quality of intra-replica sampling. As an extreme but illustrative case, consider a system of some number of frozen replicas, each with a different configuration, which undergo replica exchange moves but no conformational changes. With just a modest number of swaps, these configurations attain the probability distribution described by Eq. (13), and the hysteresis error is zero. The system has achieved inter-replica equilibrium, but the intra-replica probability distribution has not been obtained. In practice, the majority of Monte Carlo moves must be within a replica. The optimal frequency of swap moves remains an open question, although preliminary simulations suggest that more frequent swaps reduce the hysteresis error more quickly.

## VI. SUMMARY AND CONCLUSION

In a simulation of multiple replicas, each sampling the equilibrium ensemble of a different Hamiltonian, swapping configurations between replicas is a nonequilibrium work process. Accordingly, the work needed to perform such swaps has a distribution of values, as described by the Crooks fluctuation theorem. The hysteresis error  $\epsilon_H$  developed here measures how closely a given simulation reproduces these work distributions between a pair of replicas.

The hysteresis error is particularly useful in the context of free energy calculations. It reports on the combined bias of the forward and reverse free energy perturbation techniques, and it measures how completely individual replicas sample their equilibrium ensemble. The RMS hysteresis error, which reports on  $\epsilon_H$  for the whole  $\lambda$  schedule, may be decreased by running a longer simulation, employing replica exchange, utilizing an improved  $\lambda$  schedule, or all of these approaches.

The average swap probability is another useful measure and can be calculated whether or not replica exchange is employed. Since it determines the rate at which the hysteresis error decreases with simulation length, the swap probability can be used to optimize the  $\lambda$  schedule. With a uniform average swap probability the hysteresis error falls evenly between all replica pairs. This maximizes the efficiency of simulations with fixed computational resources, avoiding unnecessary replicas where the hystere-

sis is low and preventing excessive errors from regions where the hysteresis error is large.

Furthermore, the swap probability, along with a related measure  $C_\lambda$ , yields insight into the microscopic behavior of a system. The swap probability is low and  $C_\lambda$  is large when the equilibrium ensemble changes rapidly with  $\lambda$ . Slow convergence and bias errors in free energy calculations arise when there are spikes in the  $C_\lambda$  profile along the  $\lambda$  schedule, which coincides with large hysteresis errors.

### Acknowledgments

We are grateful to Hoang Tran, Albert Mao, Xiaoling Wang, Nicholas Lyle, and in particular Alan Chen and Andreas Vitalis, for helpful discussions and insightful comments. This work was supported by grants MCB - 0416766 and MCB - 0718924 from the National Science Foundation.

## APPENDIX A: DERIVATIONS

### 1. Fluctuation theorem derivation

We derive the Crooks fluctuation theorem (1) in the context of instantaneously switching  $\lambda_0 \rightarrow \lambda_1$  (forward) and  $\lambda_1 \rightarrow \lambda_0$  (reverse). Expanding the ratio  $\rho_0/\rho_1$  with (3) for an arbitrary configuration  $\Gamma$ ,

$$\begin{aligned} \frac{\rho_0(\Gamma)}{\rho_1(\Gamma)} &= \exp[\beta(F_0 - F_1) - \beta(U_0 - U_1)], \\ &= \exp(-\beta\delta F + \beta W^F), \\ &= \exp(\beta W_D^F), \end{aligned} \quad (\text{A1a})$$

and similarly,

$$\frac{\rho_1(\Gamma)}{\rho_0(\Gamma)} = \exp[\beta W_D^R(\Gamma)] \quad (\text{A1b})$$

where the definitions of work (4) and dissipated work (7) were used.

We integrate  $\rho_1$  from (A1a) over all configurations, but consider contributions only from those  $\Gamma$  for which the forward dissipated work work value takes on a specific value,  $W_D$ :

$$\begin{aligned} \int d\Gamma \rho_0(\Gamma) \exp[-\beta W_D^F(\Gamma)] \delta[\beta W_D - \beta W_D^F(\Gamma)] \\ = \int d\Gamma \rho_1(\Gamma) \delta[\beta W_D - \beta W_D^F(\Gamma)]. \end{aligned} \quad (\text{A2})$$

Since, from (A1a) and (A1b),

$$W_D^F(\Gamma) = -W_D^R(\Gamma)$$

(A2) becomes,

$$\begin{aligned} \int d\Gamma \rho_0(\Gamma) \exp[-\beta W_D^F(\Gamma)] \delta[\beta W_D - \beta W_D^F(\Gamma)] \\ = \int d\Gamma \rho_1(\Gamma) \delta[\beta W_D + \beta W_D^R(\Gamma)]. \end{aligned} \quad (\text{A3})$$

We define  $P^F(W_D)$  as the probability of observing a given dissipated work value in the forward switching process, and it can be expressed as an integral over all configurations which yield this value,

$$P^F(W_D) = \int d\Gamma \rho_0(\Gamma) \delta[\beta W_D - \beta W_D^F(\Gamma)] \quad (\text{A4a})$$

Likewise, the probability of observing a given dissipated work value in the reverse switching process is,

$$P^R(W_D) = \int d\Gamma \rho_1(\Gamma) \delta[\beta W_D - \beta W_D^R(\Gamma)] \quad (\text{A4b})$$

With these definitions, (A3) may be written as,

$$\exp(-\beta W_D) P^F(\beta W_D) = P^R(-\beta W_D),$$

which is equivalent to (1).

### 2. Fluctuation theorem and hysteresis error

The relationship between some arbitrary deviation of a simulation from the Crooks fluctuation theorem and the hysteresis error is derived by first rewriting Eq. (8) as,

$$P_R^*(-\beta W_D) \exp(\beta W_D) = P_F^*(\beta W_D) \exp(-\beta \epsilon_{FT}^*). \quad (\text{A5})$$

Inserting the  $\delta F_{FEP}^R$  definition (5b) into the definition of the hysteresis error (6), expanding the reverse work with (7b) and using the  $\delta F_{FEP}^F$  estimate for  $\delta F$ ,

$$\begin{aligned} \epsilon_H &= \delta F_{FEP}^F - \beta^{-1} \ln \langle \exp(-\beta W^R) \rangle_1^*, \\ &= \delta F_{FEP}^F - \beta^{-1} \ln [\langle \exp(-\beta W_D^R) \rangle_1^* \exp(\beta \delta F_{FEP}^F)], \\ &= -\beta^{-1} \ln [\langle \exp(-\beta W_D^R) \rangle_1^*]. \end{aligned}$$

We now expand the estimated ensemble average as an integral over all values of  $\beta W_D^R$ , with  $P_R^*$  the normalized histogram of  $\beta W_D^R$  obtained from a simulation,

$$\epsilon_H = -\beta^{-1} \ln \left[ \int_{-\infty}^{+\infty} d[\beta W_D^R] P_R^*(\beta W_D^R) \exp(-\beta W_D^R) \right].$$

As  $\beta W_D^R$  is a dummy variable, we change it to  $-\beta W_D$ ,

$$\epsilon_H = -\beta^{-1} \ln \left[ \int_{-\infty}^{+\infty} d[\beta W_D] P_R^*(-\beta W_D) \exp(\beta W_D) \right],$$

where we implicitly multiplied the integrand by  $-1$  to preserve the limits of integration. With (A5) the above can be written as,

$$\epsilon_H = -\beta^{-1} \ln \left[ \int_{-\infty}^{+\infty} d(\beta W_D) P_F^*(\beta W_D) \exp(-\beta \epsilon_{FT}^*) \right],$$

which reduces to (9).

### 3. Inter-replica equilibrium and hysteresis error

We can relate an small arbitrary error in the calculated distribution  $\rho'_N$  to the hysteresis error by considering a small error  $\rho_\epsilon(\Gamma_0, \Gamma_1)$  in the otherwise correctly estimated  $\rho'_N$ . Rewriting (13),

$$\rho'_N + \rho_\epsilon = \rho_N \exp(-\beta \Delta U_{swap}),$$

we integrate over all configuration pairs and rewrite  $\Delta U_{swap}$  with (11b),

$$\begin{aligned} & \int d\Gamma_0 d\Gamma_1 \rho'_N + \int d\Gamma_0 d\Gamma_1 \rho_\epsilon \\ &= \int d\Gamma_0 d\Gamma_1 \rho_0(\Gamma_0) \rho_1(\Gamma_1) \exp[-\beta W^F(\Gamma_0)] \\ & \times \int d\Gamma_1 \rho_1(\Gamma_1) \exp[-\beta W^R(\Gamma_1)]. \quad (A6) \end{aligned}$$

With the sampling error contained in  $\rho_\epsilon$ , the  $\rho'_N$  term (expanded with (12b)) is identically one. Taking the logarithm and dividing by  $\beta$ , (A6) becomes,

$$-\beta^{-1} \ln \left[ 1 + \int d\Gamma_0 d\Gamma_1 \rho_\epsilon \right] = \delta F_{FEP}^R - \delta F_{FEP}^F, \quad (A7)$$

where we have used the  $\delta F_{FEP}$  definitions (5). With the approximation  $\ln(1+x) \simeq x$  for small  $x$  and the definition of  $\epsilon_H$  (6), we obtain Eq. (14).

### 4. Linearized average swap probability

Here we consider the average Fermi swap probability between two replicas whose  $\lambda$  parameters differ by a small amount,  $\delta$  (written as  $\delta_\lambda$  in the text). For convenience we define

$$\begin{aligned} \mu &\equiv \beta \Delta U_{swap}, \\ &= \beta [U_\delta(\Gamma_0) - U_0(\Gamma_0) + U_0(\Gamma_\delta) - U_\delta(\Gamma_\delta)], \end{aligned}$$

where  $\Gamma_0$  and  $\Gamma_\delta$  are configurations drawn from the equilibrium distributions  $U_0$  and  $U_\delta$  parameterized by  $\lambda_0$  and  $\lambda_0 + \delta$ , respectively. We expand  $U_\delta$  as a Taylor series about  $\lambda_0$ ,

$$U_\delta(\Gamma) = U_0(\Gamma) + \delta V_0(\Gamma) + \frac{\delta^2}{2} W_0(\Gamma) + O(\delta^3),$$

with

$$\begin{aligned} V_0 &\equiv \left. \frac{\partial U}{\partial \lambda} \right|_{\lambda=\lambda_0}, \\ W_0 &\equiv \left. \frac{\partial^2 U}{\partial \lambda^2} \right|_{\lambda=\lambda_0}. \end{aligned}$$

$\mu$  can then be written as,

$$\mu = \beta \delta [V_0(\Gamma_0) - V_0(\Gamma_\delta)] + \frac{\beta \delta^2}{2} [W_0(\Gamma_0) - W_0(\Gamma_\delta)].$$

Note that  $\mu$  is small ( $O(\delta)$ ); thus, with the identities,

$$\exp(x) = 1 + x + x^2/2 + \dots, \quad (A8a)$$

$$\frac{1}{1+x} = 1 - x + x^2 - \dots, \quad (A8b)$$

we may write the Fermi swap probability between configurations  $\Gamma_0$  and  $\Gamma_\delta$  as,

$$\begin{aligned} p_{swap} &= \frac{1}{1 + \exp \mu}, \\ &= \frac{1}{2} \left( \frac{1}{1 + \mu/2 + \mu^2/4 + O(\mu^3)} \right), \\ &= \frac{1}{2} [1 - (\mu/2 + \mu^2/4) + (\mu/2 + \mu^2/4)^2 + O(\mu^3)], \\ &= \frac{1}{2} - \frac{1}{4} \mu + O(\mu^3). \end{aligned}$$

The average swap probability is the ensemble average over all configuration pairs,

$$\begin{aligned} \langle \langle p_{swap} \rangle_0 \rangle_\delta &= \frac{1}{2} - \frac{1}{4} \langle \langle \mu \rangle_0 \rangle_\delta, \\ &= \frac{1}{2} - \frac{1}{4} \left( \beta \delta \langle V_0 \rangle_0 + \frac{\beta \delta^2}{2} \langle W_0 \rangle_0 \right. \\ & \quad \left. - \beta \delta \langle V_0 \rangle_\delta - \frac{\beta \delta^2}{2} \langle W_0 \rangle_\delta \right) \\ & \quad + O(\delta^3). \quad (A9) \end{aligned}$$

To evaluate  $\langle \cdot \rangle_\delta$ , we first obtain  $Q_\delta$ , the partition function at  $(\lambda_0 + \delta)$ :

$$\begin{aligned} Q_\delta &\equiv \int d\Gamma \exp(-\beta U_\delta), \\ &= \int d\Gamma \exp(-\beta U_0) [1 - \beta \delta V_0 + O(\delta^2)], \\ &= Q_0 [1 - \beta \delta \langle V_0 \rangle_0 + O(\delta^2)], \end{aligned}$$

and its reciprocal,

$$Q_\delta^{-1} = Q_0^{-1} [1 + \beta \delta \langle V_0 \rangle_0 + O(\delta^2)].$$

We can now evaluate  $\langle V_0 \rangle_\delta$  and  $\langle W_0 \rangle_\delta$ , retaining only terms which will remain  $O(\delta^2)$  or larger in (A9):

$$\begin{aligned} \langle V_0 \rangle_\delta &\equiv Q_\delta^{-1} \int d\Gamma \exp(-\beta U_\delta) V_0, \\ &= Q_0^{-1} (1 + \beta \delta \langle V_0 \rangle_0) \int d\Gamma (1 - \beta \delta V_0) \exp(-\beta U_0) V_0, \\ &= (1 + \beta \delta \langle V_0 \rangle_0) (\langle V_0 \rangle_0 - \beta \delta \langle V_0^2 \rangle_0), \\ &= \langle V_0 \rangle_0 + \beta \delta (\langle V_0 \rangle_0^2 - \langle V_0^2 \rangle_0), \end{aligned}$$

and

$$\begin{aligned} \langle W_0 \rangle_\delta &\equiv Q_\delta^{-1} \int d\Gamma \exp(-\beta U_\delta) W_0, \\ &= Q_0^{-1} (1 + O(\delta)) \int d\Gamma \exp(-\beta U_0) W_0 [1 - O(\delta)], \\ &= \langle W_0 \rangle_0 + O(\delta). \end{aligned}$$

Finally, (A9) becomes,

$$\langle\langle p_{swap} \rangle\rangle_{\delta} = \frac{1}{2} - \frac{\beta^2 \delta^2}{4} (\langle V_0^2 \rangle_0 - \langle V_0 \rangle_0^2) + O(\delta^3), \quad (\text{A10})$$

equivalent to Eq. (18), which is valid for small  $\delta$ .

## APPENDIX B: $U_{LJ}$ AND $U_C$ FUNCTIONAL FORMS

The functional forms of both the Coulomb and Lennard-Jones potentials were developed for this work based on three criteria:

1. Configurations where the solute and solvent overlap may be observed for  $\lambda = 0$ . For such configurations, we require:
  - That swaps be permitted with reasonable frequency for small  $\lambda$  (e.g.  $\lambda = 0.1$ ).
  - That swap probabilities falls off quickly thereafter; in particular, we wish to avoid the situation where the swap probability declines only very near  $\lambda = 1.0$ .
2. We require that  $\partial U / \partial \lambda$  is not always zero for  $\lambda = 0$  to avoid complications with the Thermodynamic Integration (TI) estimator. While, we do not report results using TI in this work, we wish to construct a  $\lambda$  schedule that works with all estimators.
3. In this work,  $\lambda_{LJ} = \lambda_C$ . Therefore, Lennard-Jones repulsion must dominate Coulombic attraction at very small atomic separations.

While various ways to scale the potential have been discussed in the literature [29, 30, 31], none of these satisfied

all of our requirements. It should be noted that condition 3 is somewhat arbitrary, and more common scaled potentials may be used if the insertion process scales the Lennard-Jones prior to the Coulomb potential.

*a. Coulomb scaling* We employ a modified version of the linear soft-core scaling [30]; for two atoms of charges  $q_i$  and  $q_j$  distance  $r$  apart, the potential energy is  $\lambda_C$  as,

$$U_C(r, \lambda_C) = \lambda_C \frac{q_i q_j}{\alpha_C (1 - \lambda_C) + r}, \quad (\text{B1})$$

$\alpha_C$  controls the “soft core” term, and for small  $\lambda_C$  imposes a minimum effective atomic separation.  $\alpha_C = 1.5\text{\AA}$  for all simulations in this work.

*b. Lennard-Jones scaling* The Lennard-Jones potential between two particles may be written generally as,

$$U_{LJ}(r, \lambda_{LJ}) = BA(A - 1), \quad (\text{B2})$$

where, for unscaled Lennard-Jones,

$$A(r) = \left(\frac{\sigma}{r}\right)^6, \quad B = 4\epsilon.$$

Simple linear scaling by  $\lambda_{LJ}$  of the Lennard-Jones potential is known to be unsatisfactory, and a number of alternate forms have been introduced. We developed the exponential soft-core,

$$A(r, \lambda_{LJ}) = 1 / \left[ \alpha_{LJ} (1 - \lambda_{LJ})^b + \left(\frac{r}{\sigma}\right)^6 \right], \quad (\text{B3a})$$

$$B(\lambda_{LJ}) = 4\epsilon \frac{1 - e^{-k\lambda_{LJ}}}{1 - e^{-k}}, \quad (\text{B3b})$$

with  $a = 4$ ,  $k = 1$  and  $\alpha_{LJ} = 0.5\text{\AA}$ . The precise position along the  $\lambda$  coordinate of the swap probability trough (see Fig. 3) is specific to this Lennard-Jones potential.

- 
- |  |   |
|--|---|
| <p>[1] A. Ben-Naim, <i>Solvation Thermodynamics</i> (Plenum Press, New York, 1987).</p> <p>[2] F. M. Ytreberg, R. H. Swendsen, and D. M. Zuckerman, <i>J. Chem. Phys.</i> <b>125</b>, 184114 (2006).</p> <p>[3] R. M. Levy and E. Gallicchio, <i>Annu. Rev. Phys. Chem.</i> <b>49</b>, 531 (1998).</p> <p>[4] J. Kirkwood, <i>J. Chem. Phys.</i> <b>3</b>, 300 (1935).</p> <p>[5] D. L. Mobley, E. Dumont, J. D. Chodera, and K. A. Dill, <i>J. Phys. Chem. B</i> <b>111</b>, 2242 (2007).</p> <p>[6] N. Lu and D. A. Kofke, <i>J. Chem. Phys.</i> <b>114</b>, 7303 (2001).</p> <p>[7] D. Frenkel and B. Smit, <i>Understanding Molecular Simulation: From Algorithms to Applications</i> (Academic Press, New York, 2002).</p> <p>[8] B. Efron and R. J. Tibshirani, <i>An Introduction to the Bootstrap</i> (Chapman and Hall, New York, 1993).</p> <p>[9] D. M. Zuckerman and T. B. Woolf, <i>J. Stat. Phys.</i> <b>114</b> (2004).</p> <p>[10] G. E. Crooks, <i>Phys. Rev. E</i> <b>60</b>, 2721 (1999).</p> <p>[11] D. Chandler, <i>Introduction to Modern Statistical Mechanics</i> (Oxford University Press, New York, 1987).</p> | <p>[12] R. W. Zwanzig, <i>J. Chem. Phys.</i> <b>22</b>, 1420 (1954).</p> <p>[13] C. H. Bennett, <i>J. Comput. Phys.</i> <b>22</b>, 245 (1976).</p> <p>[14] M. R. Shirts and V. S. Pande, <i>J. Chem. Phys.</i> <b>122</b>, 144107 (2005).</p> <p>[15] Y. Sugita and Y. Okamoto, <i>Chem. Phys. Lett.</i> <b>314</b>, 141 (1999).</p> <p>[16] H. Fukunishi, O. Watanabe, and S. Takada, <i>J. Chem. Phys.</i> <b>116</b>, 9058 (2002).</p> <p>[17] C. Jarzynski, <i>Phys. Rev. E</i> <b>73</b>, 046105 (2006).</p> <p>[18] W. Jorgensen, D. Maxwell, and J. Tirado-Rives, <i>J. Am. Chem. Soc.</i> <b>118</b>, 11225 (1996).</p> <p>[19] W. Jorgensen, J. Chandrasekhar, J. Madura, R. Impey, and M. Klein, <i>J. Chem. Phys.</i> <b>79</b>, 926 (1983).</p> <p>[20] M. G. Martin and J. I. Siepmann, <i>J. Phys. Chem. B</i> <b>103</b>, 4508 (1999).</p> <p>[21] C. Predescu, M. Predescu, and C. V. Ciobanu, <i>J. Phys. Chem. B</i> <b>109</b>, 4189 (2005).</p> <p>[22] M. E. J. Newman and G. T. Barkema, <i>Monte Carlo Methods in Statistical Physics</i> (Clarendon Press, Oxford, UK, 1999).</p> |
|--|---|

- [23] H. Qian and J. J. Hopfield, *J. Chem. Phys.* **105**, 9292 (1996).
- [24] J. L. MacCallum and D. P. Tieleman, *J. Comput. Chem.* **24**, 1930 (2003).
- [25] M. R. Shirts, J. W. Pitera, W. C. Swope, and V. S. Pande, *J. Chem. Phys.* **119**, 5740 (2003).
- [26] J. Chang, A. M. Lenhoff, and S. I. Sandler, *J. Phys. Chem. B* **111**, 2098 (2007).
- [27] M. Udier-Blagović, P. M. D. Tirado, S. A. Pearlman, and W. L. Jorgensen, *J. Comput. Chem.* **25**, 1322 (2004).
- [28] R. Wolfenden, *Biochemistry* **17**, 201 (1978).
- [29] T. C. Beutler, A. E. Mark, R. C. van Scheik, P. R. Gerber, and W. F. van Gunsteren, *Chem. Phys. Lett.* **222**, 529 (1994).
- [30] J. W. Pitera and W. F. van Gunsteren, *Mol. Simulat.* **28**, 45 (2002).
- [31] M. R. Shirts and V. S. Pande, *J. Chem. Phys.* **122**, 134508 (2005).
- [32] See <http://towhee.sourceforge.net>. Version maw4\_17\_4 (maw-dev branch) was used for this work.